Design, Synthesis, and Biological Evaluation of Novel Indanones Derivatives as Potent AChE/MAO-B Inhibitors

Zhaoxin Hu[1], Shengnan Zhou[2], Junda Li[2], Xinnan Li[2], Yang Zhou[2], Zheying Zhu[3], Jinyi Xu[2,*] & Jie Liu[1,*]

[1]Department of Organic Chemistry, School of Science, China Pharmaceutical University, Nanjing, 210009, P. R. China

[2]State Key Laboratory of Natural Medicines and Department of Medicinal Chemistry, China Pharmaceutical University, 639 Longmian Avenue, Nanjing 211198, P. R. China

[3]School of Pharmacy, The University of Nottingham, University Park Campus, Nottingham NG7 2RD, U.K.

**Corresponding authors. E-mail addresses:*

jinyixu@china.com (Jinyi Xu), cpu-jill@163.com (Jie Liu)

Aim: Based on a multitarget design strategy, a series of novel indanone-1-benzyl-1,2,3,6-tetrahydropyridin hybrids were identified for the potential treatment of Alzheimer's disease (AD). **Results:** These compounds exhibited significant inhibitory activities against acetylcholinesterase (AChE) and moderate inhibitory activities toward monoamine oxidase B (MAO-B). The optimal compound **A1** possessed excellent dual AChE/MAO-B inhibition both in terms of potency (AChE: IC_{50}=0.054 ± 0.004μM; MAO-B: IC_{50}=3.25 ± 0.20μM), moderate inhibitory effects on self-mediated Aβ aggregation and

antioxidant activity. In addition, compound **A1** exhibited low neurotoxicity. More importantly, compound **A1** showed significant cognitive and spatial memory improvements in the scopolamine-induced AD mouse model. **Conclusion:** All results suggest that compound **A1** may become a promising lead of anti-AD drug for further development.

Graphical abstract:

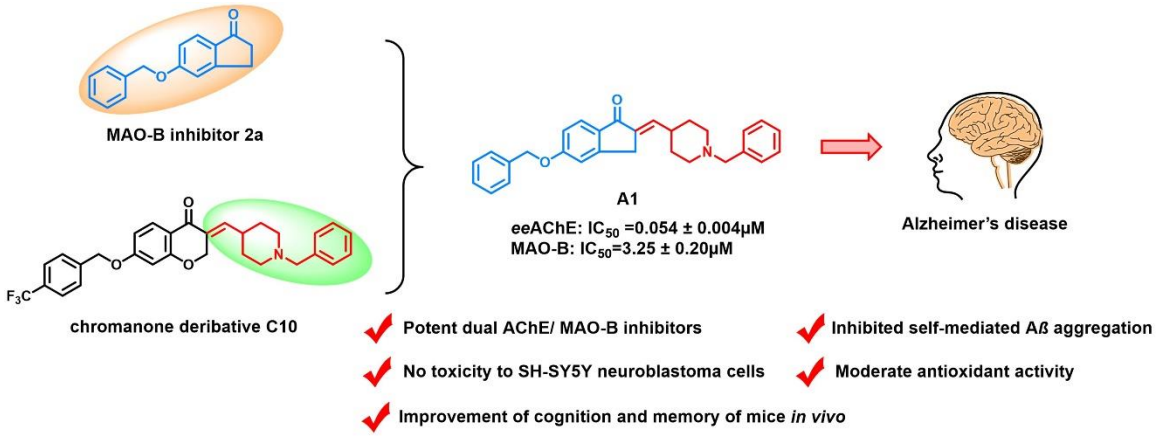

Keywords: AChE • MAO-B • MTDLs • Alzheimer's Disease • Indan-1-one

Alzheimer's disease (AD) poses a formidable challenge to treatment due to its deleterious impact on memory and executive functions, which impede daily activities[1]. Presently, the global prevalence of AD exceeds 55 million individuals, with a new case emerging every three seconds worldwide. AD is complex and multifactorial in nature[2]. The current academic community has proposed various hypotheses based on pathophysiological changes that occur during the onset and progression of AD such as Aβ aggregation[3], Tau

aggregation[4,5], metal dyshomeostasis[6], oxidative stress[7], cholinergic dysfunction[8,9], inflammation[10,11] and downregulation of autophagy[12,13].

The degree of cognitive impairment in patients with AD is completely correlated with the reductions in Acetylcholine (ACh) synthesis [10]. The remarkable decrease in ACh levels at the synaptic sites of the central nervous system is one of the distinctive features of AD. To prevent the breakdown of ACh by acetylcholinesterase (AChE), the use of AChE inhibitors can be employed. The active site of acetylcholinesterase has two vital regions. One is the catalytic active site (CAS), which is made up of three amino acid residues: Ser203, His447 and Glu334[14]. CAS is located at the bottom of the enzyme active pocket and plays a catalytic role. The other region is the peripheral anionic site (PAS), near the entrance of the gorge, which consists of five amino acid residues: Tyr 72, Tyr124, Trp286, Tyr341 and Asp74. The dual-site AChE inhibitors with both the CAS and PAS are of great significance for the prevention of AD. The Food and Drug Administration (FDA) has approved four AChE inhibitors, namely tacrine, donepezil, rivastigmine and galantamine. However, the first AChE inhibitor, tacrine, was discontinued due to concerns linked to hepatotoxicity[15,16].

Aβ antibodies are a treatment for improving cognitive impairment, and aducanumab and lecanemab have been approved by the FDA for targeting Aβ

plaques[17]. However, the approval of aducanumab was met with controversy due to unclear treatment efficacy, particularly as previous clinical trials have shown that soluble Aβ antibodies can exacerbate cognitive decline in patients with AD[18]. The production cost of small molecule drugs is generally lower compared to antibodies, and they can often be administered orally. Therefore, the development of small molecule drugs against AD remains an effective strategy for the treatment of cognitive impairment.

However, the progression of AD can't be stopped or reversed by single targets of small molecule drugs because of the compensatory effects of other morbid signaling pathways, and a multitarget strategy possesses a more effective and promising capacity to manage the special disease network of AD with synergistic adjustment towards more pivotal targets for the potentially curable treatment of AD.

Monoamine oxidases (MAO) are flavin adenine dinucleotide (FAD) containing enzymes localized on the mitochondrial outer membrane which has two subtypes: MAO-A and MAO-B[19]. The X-ray crystal structures of human MAO-B and human MAO-A were reported in 2002 and 2005, respectively[20]. A unique structural feature is that the crystal of human MAO-A is a monomeric unit, but the crystals of rat MAO-A and human MAO-B are dimers[21]. MAO-B inhibitors can be used to treat other neurodegenerative diseases as well including Parkinson's disease (PD) and

Alzheimer's disease[22,23]. Various studies have reported that MAO-B is overexpressed in the brain of AD patients and is linked with the loss of cognitive functions[24,25]. The brains of patients with AD exhibit high levels of MAO-B activity, causing an increase in dopamine metabolism that generates excessive amounts of hydrogen peroxide, ultimately resulting in nerve damage. Thus, inhibition of MAO-B may prevent oxidative stress from damaging the nervous system and has derived from neuroprotective effects[26,27].

The pathogenesis of AD is complex, which makes existing single-target drugs effective only in relieving mild to moderate AD symptoms but unable to halt the progression of the disease. Single-target directed drugs are not suitable for the treatment of AD with complex pathogenesis; therefore, the study of novel multi-target directed ligands (MTDLs) targeting different targets or mechanisms of AD may be a more effective approach[8,28]. There is much literature had shown that compounds with dual inhibitory activities for AChE and MAO-B have the potential to be used in the treatment of Alzheimer's disease[29–32].

Mostert et al. reported a series of MAO-B inhibitors, among which compound **2a** demonstrated potent MAO-B inhibitory activity (IC_{50}=0.135 ± 0.007μM) and high selectivity (MAO-A: IC_{50}=10.75 ± 0.799μM; MAO-B:

IC_{50}=0.135 ± 0.007μM)[33]. Indan-1-one， the scaffold of compound **2a**， is a very important scaffold of organic compounds, and many natural products and drug molecules contain indan-1-one structural units. In our previous work, we reported a novel chromanone derivative **C10**, which is an AChE/MAO-B inhibitor with excellent dual inhibition[34] (*ee*AChE: IC_{50}=0.58 ± 0.05μM; MAO-B: IC_{50}=0.135 ± 0.007μM). Therefore, we continue to use the strategy of MTDLs to design and synthesize inhibitors with dual inhibitory effects of AChE and MAO-B. As shown in Figure 1, we selected Indan-1-one as the scaffold, and incorporated the structure of chromanone derivative **C10** and the MAO-B inhibitor **2a**, to obtain a series of novel MTDLs containing indanone-1-benzyl-1,2,3,6-tetrahydropyridin (**A1-A10, B1-B18**), with the yield higher affinity at both targets (Figure 1).

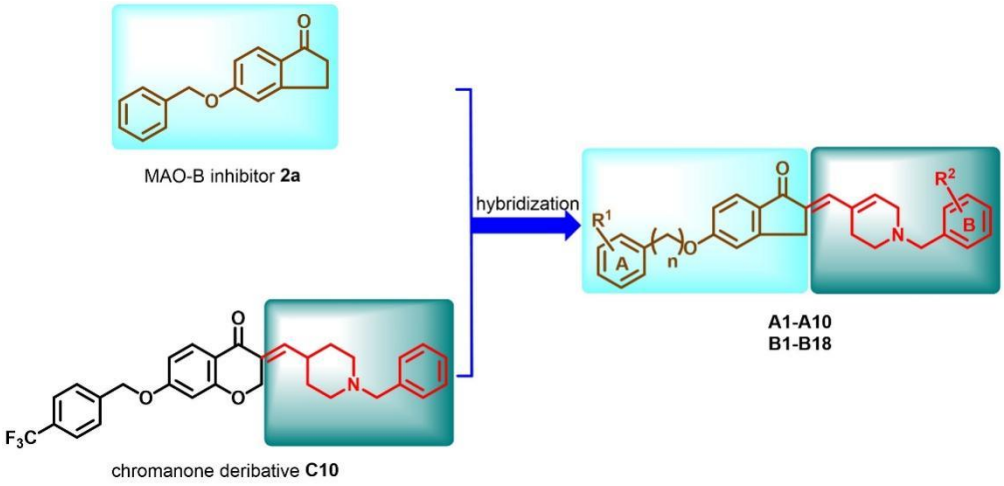

Figure 1. Design of novel dual AChE/MAO-B inhibitors **A1−A10** and **B1−B18**.

The AD market is a blue ocean, yet the availability of approved drugs remains limited, leaving a significant unmet demand in the

treatment of AD field. Although numerous novel drugs are currently being investigated in clinical research, there is still a lack of AD new drugs with multi-target efficacy. In response to this issue, based on our previous work, we further designed and synthesized a series of new AChE/MAO-B inhibitors featuring a novel indanone scaffold. Significantly, the novel indanone scaffold derivatives exhibited excellent dual inhibitory activity, which will provide valuable insights for future researchers. There is no shortcut to overcoming AD, but MTDLs may offer hope for the treatment of AD[35].

Materials & methods

Chemistry

All starting materials and reference compounds were obtained from commercial sources and do not require further purification. The ^{1}H NMR and ^{13}C NMR spectra were acquired using a Bruker BioSpin GmbH spectrometer (Bruker, Germany) operating at frequencies of either 300 or 400 MHz for the former and either 75 or 100 MHz for the latter. The solvents employed were $CDCl_3$ or DMSO-d_6. Tetramethylsilane was utilized as the reference standard, with chemical shifts reported in parts per million (ppm), coupling constants J given in Hertz (Hz), and spin multiplicities denoted by singlet (s), broad singlet (brs), doublet (d), doublet of doublets (dd), triplet (t) and multiplet (m). All reagents employed in this study were commercially available and of

chemically pure or analytical grade. Dry acetonitrile (MeCN) is treated with anhydrous magnesium sulfate and left to stand overnight. Anhydrous methanol (MeOH) and ethanol (EtOH), both commercially available as anhydrous solvents, are used directly. Other solvents are not treated and should be used directly unless otherwise specified. The reactions were routinely monitored via thin-layer chromatography on silica gel and visualized under a 254 nm UV light source. The representative compounds were determined to have a purity of ⩾95% through HPLC analysis (SHIMADZU Lab solutions, UV detection at λ = 254 nm) on an Agilent C18 column (4.6 × 150 mm, 5 mm), with elution using acetonitrile and water (70:30) at a flow rate of 1 mL/min.

Synthesis of Intermediates ***3-1~3-10.*** To a solution of 5-hydroxy-2,3-dihydro-1*H*-inden-1-one (1) (1 mmol) and benzyl bromide with different substituted (**2-1~2-10**) in 10ml of *N, N*-dimethylformamide, potassium carbonate (2 mmol) was added and stirred at 65℃ for 2 h. Upon detection of completion of the reaction by TLC, the mixture was subjected to extraction with ethyl acetate (3 × 100 mL). The combined organic layers were subsequently washed with brine (200 mL), dried over anhydrous Na_2SO_4, and finally purified via flash column chromatography to yield white solid intermediates **3-1~3-10**.

Synthesis of Intermediates ***4-1~4-10.*** To a solution of intermediates **3-1~3-10**

(1 mmol) and 4-pyridinecarboxaldehyde (1.5 mmol) in 20 mL of toluene, *p*-toluenesulfonic acid monohydrate (2 mmol) was added. The mixture was refluxed for 4 h. Upon detection of completion of the reaction by TLC, the mixture was subjected to extraction with ethyl acetate (3 × 100 mL). The combined organic layers were subsequently washed with brine (200 mL), dried over anhydrous Na_2SO_4, and finally purified via flash column chromatography to yield white solid intermediates **4-1~4-10**.

Synthesis of Intermediates ***5-1~5-10.*** To a solution of intermediates **4-1~4-10** (1 mmol) in 10 mL of acetonitrile, benzyl bromide (1.1 mmol) was added. The mixture was refluxed for 3 h. After being cooled to room temperature, the mixture was filtered and the resulting solid was washed three times with ethyl acetate. The crude intermediates **5-1~5-10** were utilized in the subsequent step without undergoing purification.

Synthesis of Compounds ***A1~A10.*** To a solution of intermediates **5-1~5-10** (1 mmol) in 10 mL of methanol, sodium borohydride (1 mmol) was slowly added and the mixture was stirred at -5°C for 1 hour. Upon completion of the reaction, the mixture was extracted with ethyl acetate (3 × 100 mL). The combined organic layers were dried over anhydrous Na_2SO_4 and purified by flash column chromatography to yield target compounds **A1~A10**.

*(E)-2-((1-benzyl-1,2,3,6-tetrahydropyridin-4-yl)methylene)-5-(benzyloxy)-2,3-dihydro-1H-inden-1-one(**A1**).* White solid, yield 40.3%, mp 102-104 °C.

^{1}H NMR (300 MHz, Chloroform-*d*) δ 7.81 (d, J = 8.3 Hz, 1H), 7.46 – 7.40 (m, 4H), 7.39 – 7.30 (m, 6H), 7.17 (s, 1H), 7.03 – 6.96 (m, 2H), 6.23 (t, J = 3.8 Hz, 1H), 5.15 (s, 2H), 3.85 (s, 2H), 3.63 (s, 2H), 3.20 (d, J = 3.4 Hz, 2H), 2.68 (dd, J = 6.2, 3.8 Hz, 2H), 2.62 (s, 2H). ^{13}C NMR (75 MHz, Chloroform-*d*) δ 164.12, 152.47, 137.87, 136.11, 134.93, 134.01, 132.59, 131.80, 129.21, 128.76, 128.37, 128.32, 127.51, 127.28, 126.07, 115.81, 110.54, 70.35, 62.59, 53.76, 49.50, 31.94, 28.22. ^{13}C NMR (75 MHz, $CDCl_3$) δ 193.08, 164.12, 152.47, 137.87, 136.11, 135.99, 134.93, 134.01, 132.59, 131.80, 129.21, 128.76, 128.37, 128.32, 127.51, 127.28, 126.07, 115.81, 110.54, 70.35, 62.59, 53.76, 49.50, 31.94, 28.22. HR-MS (ESI) m/z: calcd for $C_{29}H_{27}NO_2$ $[M + H]^+$, 422.2115; found, 422.2121.

*(E)-2-((1-benzyl-1,2,3,6-tetrahydropyridin-4-yl)methylene)-5-phenethoxy-2,3-dihydro-1H-inden-1-one(**A2**).* White solid, yield 43.8%, mp 136-138 °C. ^{1}H NMR (300 MHz, Chloroform-*d*) δ 7.79 (d, J = 8.3 Hz, 1H), 7.40 – 7.27 (m, 10H), 7.16 (s, 1H), 6.94 – 6.88 (m, 2H), 6.22 (t, J = 3.8 Hz, 1H), 4.25 (t, J = 7.0 Hz, 2H), 3.84 (s, 2H), 3.63 (s, 2H), 3.23 – 3.17 (m, 2H), 3.13 (t, J = 7.0 Hz, 2H), 2.67 (t, J = 4.8 Hz, 2H), 2.61 (d, J = 5.6 Hz, 2H). ^{13}C NMR (75 MHz, $CDCl_3$) δ 193.12, 164.25, 152.50, 137.90, 137.79, 135.98, 134.88, 134.02, 132.62, 131.60, 129.23, 129.03, 128.62, 128.38, 127.29, 126.72, 126.04, 115.59, 110.10, 69.07, 62.63, 53.80, 49.52, 35.63, 31.91, 28.22. MS (ESI) m/z: calcd for $C_{30}H_{29}NO_2$ $[M + H]^+$, 436.2; found, 436.2.

*(E)-2-((1-benzyl-1,2,3,6-tetrahydropyridin-4-yl)methylene)-5-(3-phenylpropoxy)-2,3-dihydro-1H-inden-1-one(**A3**)*. White solid, yield 46.5%, mp 140-142 °C. ^{1}H NMR (300 MHz, Chloroform-*d*) δ 7.79 (d, J = 8.5 Hz, 1H), 7.36 – 7.26 (m, 7H), 7.23 – 7.16 (m, 4H), 6.94 – 6.86 (m, 2H), 6.21 (d, J = 3.9 Hz, 1H), 4.03 (t, J = 6.2 Hz, 2H), 3.84 (s, 2H), 3.64 (s, 2H), 3.21 (q, J = 3.0 Hz, 2H), 2.82 (t, J = 7.5 Hz, 2H), 2.69 (t, J = 5.0 Hz, 2H), 2.62 (d, J = 5.7 Hz, 2H), 2.17 – 2.11 (m, 2H). ^{13}C NMR (101 MHz, $CDCl_3$) δ 193.08, 164.49, 152.49, 141.17, 134.74, 134.02, 132.71, 131.50, 129.24, 128.53, 128.51, 128.38, 127.32, 126.09, 126.02, 115.57, 110.04, 67.28, 62.57, 53.71, 49.49, 32.05, 31.92, 30.62, 28.19. MS (ESI) m/z: calcd for $C_{31}H_{31}NO_2$ $[M + H]^+$, 450.2; found, 450.2.

*(E)-2-((1-benzyl-1,2,3,6-tetrahydropyridin-4-yl)methylene)-5-((2-fluorobenzyl)oxy)-2,3-dihydro-1H-inden-1-one(**A4**)*. White solid, yield 47.6%, mp 136-138 °C. ^{1}H NMR (300 MHz, Chloroform-*d*) δ 7.86 – 7.78 (m, 1H), 7.49 (t, J = 7.5 Hz, 1H), 7.38 – 7.28 (m, 6H), 7.21 – 7.11 (m, 3H), 7.01 (d, J = 7.5 Hz, 2H), 6.24 (s, 1H), 5.22 (s, 2H), 3.87 (s, 2H), 3.63 (s, 2H), 3.21 (s, 2H), 2.68 (t, J = 4.8 Hz, 2H), 2.62 (s, 2H). ^{13}C NMR (101 MHz, $CDCl_3$) δ 193.04, 163.84, 152.47, 134.99, 134.01, 132.54, 131.98, 130.15, 130.07, 129.73, 129.69, 129.18, 128.35, 127.25, 126.09, 124.43, 124.40, 115.77, 115.62, 115.41, 110.43, 64.04, 62.60, 53.78, 49.51, 31.95, 28.25. MS (ESI) m/z: calcd for $C_{29}H_{26}FNO_2$ $[M + H]^+$, 440.2; found, 440.2.

*(E)-2-((1-benzyl-1,2,3,6-tetrahydropyridin-4-yl)methylene)-5-((3-fluorobenzyl)oxy)-2,3-dihydro-1H-inden-1-one(**A15**)*. White solid, yield 44.2%, mp 138-140 °C. ^{1}H NMR (300 MHz, Chloroform-*d*) δ 7.81 (d, J = 8.4 Hz, 1H), 7.41 – 7.30 (m, 6H), 7.23 – 7.14 (m, 3H), 7.06 – 6.94 (m, 3H), 6.23 (d, J = 4.0 Hz, 1H), 5.13 (s, 2H), 3.85 (s, 2H), 3.63 (s, 2H), 3.20 (q, J = 2.9 Hz, 2H), 2.67 (t, J = 4.8 Hz, 2H), 2.61 (d, J = 5.4 Hz, 2H). ^{13}C NMR (101 MHz, $CDCl_3$) δ 193.00, 163.75, 152.44, 138.76, 138.68, 137.94, 136.12, 135.04, 134.00, 132.49, 132.02, 130.37, 130.29, 129.18, 128.36, 127.26, 126.11, 122.74, 122.71, 115.72, 115.27, 115.06, 114.36, 114.14, 110.58, 69.48, 62.60, 53.79, 49.50, 31.94, 28.25. MS (ESI) m/z: calcd for $C_{29}H_{26}FNO_2$ [M + H]+, 440.2; found, 440.2.

*(E)-2-((1-benzyl-1,2,3,6-tetrahydropyridin-4-yl)methylene)-5-((4-fluorobenzyl)oxy)-2,3-dihydro-1H-inden-1-one(**A16**)*. White solid, yield 43.6%, mp 138-140 °C. ^{1}H NMR (400 MHz, Chloroform-*d*) δ 7.81 (d, J = 8.4 Hz, 1H), 7.46 – 7.29 (m, 7H), 7.17 (s, 1H), 7.09 (t, J = 8.5 Hz, 2H), 7.01 – 6.93 (m, 2H), 6.22 (d, J = 4.1 Hz, 1H), 5.09 (s, 2H), 3.85 (s, 2H), 3.63 (s, 2H), 3.27 – 3.14 (m, 2H), 2.67 (t, J = 5.5 Hz, 2H), 2.61 (d, J = 5.7 Hz, 2H). ^{13}C NMR (101 MHz, $CDCl_3$) δ 193.06, 163.91, 152.47, 137.86, 136.11, 135.02, 134.00, 132.52, 131.89, 131.85, 129.46, 129.38, 129.21, 128.37, 127.29, 126.09, 115.81, 115.74, 115.59, 110.51, 69.65, 62.60, 53.77, 49.49, 31.93, 28.21. MS (ESI) m/z: calcd for $C_{29}H_{26}FNO_2$ $[M + H]^+$, 440.2; found, 440.2.

*(E)-2-((1-benzyl-1,2,3,6-tetrahydropyridin-4-yl)methylene)-5-((4-chlorobenzyl)oxy)-2,3-dihydro-1H-inden-1-one(**A7**).* White solid, yield 43.4%, mp 140-142 °C. ^{1}H NMR (300 MHz, Chloroform-*d*) δ 7.81 (d, J = 8.4 Hz, 1H), 7.41 – 7.29 (m, 9H), 7.17 (s, 1H), 7.01 – 6.93 (m, 2H), 6.24 (d, J = 4.1 Hz, 1H), 5.11 (s, 2H), 3.85 (s, 2H), 3.63 (s, 2H), 3.26 – 3.16 (m, 2H), 2.67 (t, J = 5.7 Hz, 2H), 2.62 (s, 2H). ^{13}C NMR (101 MHz, $CDCl_3$) δ 193.05, 163.80, 152.46, 137.86, 136.13, 135.06, 134.61, 134.14, 133.99, 132.49, 131.96, 129.21, 128.94, 128.80, 128.37, 127.29, 126.11, 115.74, 110.54, 69.53, 62.59, 53.77, 49.48, 31.93, 28.21. MS (ESI) m/z: calcd for $C_{29}H_{26}ClNO_2$ $[M + H]^+$, 456.2; found, 456.2.

*(E)-2-((1-benzyl-1,2,3,6-tetrahydropyridin-4-yl)methylene)-5-((4-bromobenzyl)oxy)-2,3-dihydro-1H-inden-1-one(**A8**).* White solid, yield 41.6%, mp 144-146 °C. ^{1}H NMR (300 MHz, Chloroform-*d*) δ 7.81 (d, J = 8.4 Hz, 1H), 7.56 – 7.51 (m, 2H), 7.38 – 7.28 (m, 7H), 7.17 (s, 1H), 7.01 – 6.92 (m, 2H), 6.23 (t, J = 3.9 Hz, 1H), 5.09 (s, 2H), 3.85 (s, 2H), 3.63 (s, 2H), 3.20 (q, J = 2.8 Hz, 2H), 2.67 (t, J = 4.9 Hz, 2H), 2.61 (d, J = 5.4 Hz, 2H). ^{13}C NMR (75 MHz, $CDCl_3$) δ 193.03, 163.78, 152.45, 137.88, 136.13, 135.15, 135.05, 133.99, 132.48, 131.98, 131.89, 129.20, 129.07, 128.37, 127.28, 126.11, 122.25, 115.74, 110.55, 69.55, 62.60, 53.77, 49.49, 31.93, 28.22. MS (ESI) m/z: calcd for $C_{29}H_{26}BrNO_2$ $[M + H]^+$, 500.1; found, 500.1.

(E)-2-((1-benzyl-1,2,3,6-tetrahydropyridin-4-yl)methylene)-5-((4-

*methylbenzyl)oxy)-2,3-dihydro-1H-inden-1-one(**A9**)*. White solid, yield 49.5%, mp 140-142 °C. ^{1}H NMR (300 MHz, Chloroform-*d*) δ 7.80 (d, J = 8.3 Hz, 1H), 7.38 – 7.29 (m, 7H), 7.23 – 7.16 (m, 3H), 6.99 (d, J = 8.8 Hz, 2H), 6.25 – 6.20 (m, 1H), 5.10 (s, 2H), 3.85 (s, 2H), 3.63 (s, 2H), 3.20 (d, J = 3.5 Hz, 2H), 2.68 (t, J = 5.5 Hz, 2H), 2.62 (s, 2H), 2.37 (s, 3H). ^{13}C NMR (75 MHz, $CDCl_3$) δ 193.18, 164.26, 152.54, 138.25, 137.93, 136.08, 134.96, 134.07, 133.08, 132.66, 131.74, 129.50, 129.28, 128.43, 127.74, 127.34, 126.09, 115.90, 110.55, 70.35, 62.66, 53.82, 49.55, 32.00, 28.26, 21.34. MS (ESI) m/z: calcd for $C_{30}H_{29}NO_2$ $[M + H]^+$, 436.2; found, 436.2.

*(E)-2-((1-benzyl-1,2,3,6-tetrahydropyridin-4-yl)methylene)-5-((4-(trifluoromethyl)benzyl)oxy)-2,3-dihydro-1H-inden-1-one(**A10**).* White solid, yield 48.2%, mp 144-146 °C. ^{1}H NMR (400 MHz, Chloroform-*d*) δ 7.82 (d, J = 8.4 Hz, 1H), 7.66 (d, J = 8.1 Hz, 2H), 7.55 (d, J = 8.0 Hz, 2H), 7.37 – 7.28 (m, 5H), 7.17 (s, 1H), 7.03 – 6.94 (m, 2H), 6.23 (t, J = 3.9 Hz, 1H), 5.20 (s, 2H), 3.85 (s, 2H), 3.63 (s, 2H), 3.20 (q, J = 3.0 Hz, 2H), 2.66 (d, J = 5.2 Hz, 2H), 2.64 – 2.58 (m, 2H). ^{13}C NMR (101 MHz, $CDCl_3$) δ 193.02, 163.62, 152.48, 140.18, 137.88, 136.25, 135.15, 133.98, 132.41, 132.11, 129.20, 128.37, 127.40, 127.28, 126.16, 125.77, 125.73, 125.70, 125.66, 115.70, 110.55, 69.39, 62.61, 53.79, 49.49, 31.93, 28.22. MS (ESI) m/z: calcd for $C_{30}H_{26}F_3NO_2$ $[M + H]^+$, 490.2; found, 490.2.

*Synthesis of Intermediates **6-1~6-18.*** To a solution of intermediates **4-1** (1

mmol) in 10 mL of acetonitrile, benzyl bromide with different substituted (**5-1~5-18**) (1.1 mmol) was added. The mixture was refluxed for 3 h. After being cooled to room temperature, the mixture was filtered and the resulting solid was washed three times with ethyl acetate. The crude intermediates **6-1~6-18** were utilized in the subsequent step without undergoing purification.

*Synthesis of Compounds **B1~B18.*** To a solution of intermediates **6-1~6-18** (1 mmol) in 10 mL of methanol, sodium borohydride (1 mmol) was slowly added and the mixture was stirred at -5°C for 1 hour. Upon completion of the reaction, the mixture was extracted with ethyl acetate (3 × 100 mL). The combined organic layers were dried over anhydrous Na_2SO_4 and purified by flash column chromatography to yield target compounds **B1~B18**.

*(E)-5-(benzyloxy)-2-((1-(2-fluorobenzyl)-1,2,3,6-tetrahydropyridin-4-yl)methylene)-2,3-dihydro-1H-inden-1-one(**B1**).* White solid, yield 43.9%, mp 116-118 °C. ^{1}H NMR (400 MHz, Chloroform-*d*) δ 7.80 (d, J = 8.4 Hz, 1H), 7.46 – 7.28 (m, 7H), 7.13 (dd, J = 13.7, 6.1 Hz, 2H), 7.07 – 6.96 (m, 3H), 6.21 (d, J = 3.9 Hz, 1H), 5.14 (s, 2H), 3.84 (s, 2H), 3.70 (s, 2H), 3.24 (d, J = 3.5 Hz, 2H), 2.71 (t, J = 5.6 Hz, 2H), 2.62 (d, J = 6.1 Hz, 2H). ^{13}C NMR (75 MHz, $CDCl_3$) δ 193.15, 164.21, 152.56, 136.20, 135.96, 134.96, 134.02, 132.71, 131.87, 131.69, 131.64, 129.15, 129.04, 128.85, 128.41, 127.60, 126.15, 124.13, 124.08, 115.91, 115.60, 115.30, 110.62, 70.43, 54.86, 53.47, 49.53, 32.02, 28.32. MS (ESI) m/z: calcd for $C_{29}H_{26}FNO_2$ $[M + H]^+$, 440.2;

found, 440.2.

*(E)-5-(benzyloxy)-2-((1-(3-fluorobenzyl)-1,2,3,6-tetrahydropyridin-4-yl)methylene)-2,3-dihydro-1H-inden-1-one(**B2**).* White solid, yield 40.6%, mp 118-120 °C. ^{1}H NMR (300 MHz, Chloroform-*d*) δ 7.81 (d, J = 8.3 Hz, 1H), 7.35 (dd, J = 19.8, 11.5 Hz, 6H), 7.13 (dd, J = 15.4, 9.2 Hz, 3H), 7.00 (d, J = 10.6 Hz, 3H), 6.22 (s, 1H), 5.14 (s, 2H), 3.85 (s, 2H), 3.61 (s, 2H), 3.20 (s, 2H), 2.81 – 2.47 (m, 4H). ^{13}C NMR (75 MHz, $CDCl_3$) δ 193.05, 164.15, 152.47, 136.13, 135.80, 134.82, 134.04, 132.69, 131.80, 129.84, 129.74, 128.78, 128.34, 127.52, 126.08, 124.55, 115.84, 115.62, 114.27, 113.99, 110.55, 70.36, 61.98, 53.77, 49.54, 31.95, 28.24. MS (ESI) m/z: calcd for $C_{29}H_{26}FNO_2$ $[M + H]^+$, 440.2; found, 440.2.

*(E)-5-(benzyloxy)-2-((1-(4-fluorobenzyl)-1,2,3,6-tetrahydropyridin-4-yl)methylene)-2,3-dihydro-1H-inden-1-one(**B3**).* White solid, yield 39.6%, mp 118-120 °C. ^{1}H NMR (300 MHz, Chloroform-*d*) δ 7.80 (d, J = 8.4 Hz, 1H), 7.45 – 7.35 (m, 5H), 7.33 – 7.27 (m, 2H), 7.16 (s, 1H), 7.05 – 6.97 (m, 4H), 6.21 (d, J = 3.9 Hz, 1H), 5.13 (s, 2H), 3.84 (s, 2H), 3.58 (s, 2H), 3.17 (d, J = 3.6 Hz, 2H), 2.65 (dd, J = 7.9, 3.6 Hz, 2H), 2.60 (d, J = 6.8 Hz, 2H). ^{13}C NMR (75 MHz, $CDCl_3$) δ 193.26, 164.29, 152.65, 136.24, 136.07, 135.03, 134.19, 133.85, 133.81, 132.80, 131.90, 130.88, 130.77, 128.93, 128.50, 127.68, 126.23, 116.00, 115.48, 115.19, 110.67, 70.49, 61.94, 53.88, 49.58, 32.10, 28.36. MS (ESI) m/z: calcd for $C_{29}H_{26}FNO_2$ $[M + H]^+$, 440.2; found,

440.2.

*(E)-5-(benzyloxy)-2-((1-(2-chlorobenzyl)-1,2,3,6-tetrahydropyridin-4-yl)methylene)-2,3-dihydro-1H-inden-1-one(**B4**)*. White solid, yield 43.4%, mp 126-128 °C. ^{1}H NMR (400 MHz, Chloroform-*d*) δ 7.79 (d, J = 8.4 Hz, 1H), 7.50 (dd, J = 7.5, 1.9 Hz, 1H), 7.45 – 7.38 (m, 4H), 7.38 – 7.34 (m, 2H), 7.25 – 7.22 (m, 1H), 7.20 (dd, J = 7.6, 2.0 Hz, 1H), 7.15 (d, J = 2.2 Hz, 1H), 6.98 (dd, J = 8.4, 2.3 Hz, 1H), 6.96 (d, J = 2.1 Hz, 1H), 6.27 – 6.15 (m, 1H), 5.12 (s, 2H), 3.82 (d, J = 2.1 Hz, 2H), 3.73 (s, 2H), 3.26 (q, J = 3.0 Hz, 2H), 2.71 (t, J = 5.6 Hz, 2H), 2.60 (p, J = 4.6, 3.7 Hz, 2H). ^{13}C NMR (101 MHz, $CDCl_3$) δ 192.97, 164.05, 152.43, 136.06, 136.04, 135.73, 134.84, 134.26, 133.94, 132.54, 131.71, 130.62, 129.46, 128.70, 128.26, 127.45, 126.69, 125.97, 115.76, 110.46, 70.26, 58.75, 53.72, 49.63, 31.89, 28.22. MS (ESI) m/z: calcd for $C_{29}H_{26}ClNO_2$ $[M + H]^+$, 456.2; found, 456.2.

*(E)-5-(benzyloxy)-2-((1-(3-chlorobenzyl)-1,2,3,6-tetrahydropyridin-4-yl)methylene)-2,3-dihydro-1H-inden-1-one(**B5**)*. White solid, yield 41.6%, mp 124-126 °C. ^{1}H NMR (300 MHz, Chloroform-*d*) δ 7.82 (d, J = 8.3 Hz, 1H), 7.40 (dd, J = 12.6, 4.3 Hz, 7H), 7.25 (d, J = 1.6 Hz, 2H), 7.18 (s, 1H), 7.05 – 6.97 (m, 2H), 6.23 (s, 1H), 5.15 (s, 2H), 3.87 (s, 2H), 3.59 (s, 2H), 3.20 (d, J = 3.5 Hz, 2H), 2.65 (d, J = 5.6 Hz, 2H). ^{13}C NMR (75 MHz, $CDCl_3$) δ 193.34, 164.39, 152.72, 140.44, 136.33, 135.98, 135.06, 134.54, 134.27, 132.94, 132.01, 129.89, 129.31, 129.02, 128.59, 127.77, 127.71, 127.45,

126.34, 116.08, 110.78, 70.59, 62.21, 54.00, 49.77, 32.20, 28.43. MS (ESI) m/z: calcd for $C_{29}H_{26}ClNO_2$ $[M + H]^+$, 456.2; found, 456.2.

*(E)-5-(benzyloxy)-2-((1-(4-chlorobenzyl)-1,2,3,6-tetrahydropyridin-4-yl)methylene)-2,3-dihydro-1H-inden-1-one(**B6**).* White solid, yield 45.1%, mp 122-124 °C. ^{1}H NMR (300 MHz, Chloroform-*d*) δ 7.81 (d, J = 8.3 Hz, 1H), 7.42 (d, J = 6.3 Hz, 4H), 7.38 – 7.34 (m, 1H), 7.30 (s, 4H), 7.17 (s, 1H), 7.05 – 6.95 (m, 2H), 6.22 (s, 1H), 5.15 (s, 2H), 3.85 (s, 2H), 3.58 (s, 2H), 3.18 (d, J = 3.9 Hz, 2H), 2.64 (dd, J = 9.5, 5.4 Hz, 4H). ^{13}C NMR (75 MHz, $CDCl_3$) δ 192.97, 164.08, 152.39, 136.49, 136.03, 135.69, 134.73, 133.96, 132.90, 132.63, 131.70, 130.35, 128.70, 128.45, 128.27, 127.44, 126.01, 115.78, 110.47, 70.28, 61.71, 53.67, 49.39, 31.88, 28.14. MS (ESI) m/z: calcd for $C_{29}H_{26}ClNO_2$ $[M + H]^+$, 456.2; found, 456.2.

*(E)-5-(benzyloxy)-2-((1-(2-bromobenzyl)-1,2,3,6-tetrahydropyridin-4-yl)methylene)-2,3-dihydro-1H-inden-1-one(**B7**).* White solid, yield 43.2%, mp 126-128 °C. ^{1}H NMR (300 MHz, Chloroform-*d*) δ 7.81 (d, J = 8.3 Hz, 1H), 7.54 (ddd, J = 13.8, 7.8, 3.6 Hz, 2H), 7.44 – 7.26 (m, 7H), 7.16 – 7.10 (m, 1H), 7.03 – 6.97 (m, 2H), 6.25 (d, J = 3.7 Hz, 1H), 5.15 (s, 2H), 3.87 (s, 2H), 3.73 (s, 2H), 3.29 (d, J = 3.5 Hz, 2H), 2.74 (t, J = 5.6 Hz, 2H), 2.64 (d, J = 5.5 Hz, 2H). ^{13}C NMR (75 MHz, $CDCl_3$) δ 193.09, 164.15, 152.49, 137.45, 136.13, 136.08, 134.94, 134.04, 132.84, 132.64, 131.82, 130.72, 128.79, 128.62, 128.35, 127.54, 127.40, 126.11, 124.69, 115.83, 110.58, 70.38, 61.35,

53.78, 49.71, 32.00, 28.32. MS (ESI) m/z: calcd for $C_{29}H_{26}BrNO_2$ $[M + H]^+$, 500.1; found, 500.1.

*(E)-5-(benzyloxy)-2-((1-(3-bromobenzyl)-1,2,3,6-tetrahydropyridin-4-yl)methylene)-2,3-dihydro-1H-inden-1-one(**B8**).* White solid, yield 41.4%, mp 126-128 °C. ^{1}H NMR (300 MHz, Chloroform-*d*) δ 7.81 (d, J = 8.3 Hz, 1H), 7.53 (s, 1H), 7.47 – 7.35 (m, 7H), 7.23 – 7.14 (m, 2H), 7.00 (d, J = 10.1 Hz, 2H), 6.22 (s, 1H), 5.15 (s, 2H), 3.86 (s, 2H), 3.59 (s, 2H), 3.19 (s, 2H), 2.64 (t, J = 6.2 Hz, 4H). ^{13}C NMR (75 MHz, $CDCl_3$) δ 193.07, 164.17, 152.48, 140.52, 136.11, 135.67, 134.79, 134.03, 132.74, 131.97, 131.78, 130.41, 129.96, 128.77, 128.34, 127.68, 127.52, 126.10, 122.59, 115.85, 110.56, 70.35, 61.89, 53.73, 49.52, 31.95, 28.18. MS (ESI) m/z: calcd for $C_{29}H_{26}BrNO_2$ $[M + H]^+$, 500.1; found, 500.1.

*(E)-5-(benzyloxy)-2-((1-(4-bromobenzyl)-1,2,3,6-tetrahydropyridin-4-yl)methylene)-2,3-dihydro-1H-inden-1-one(**B9**).* White solid, yield 43.5%, mp 128-130 °C. ^{1}H NMR (300 MHz, Chloroform-*d*) δ 7.80 (d, J = 8.3 Hz, 1H), 7.51 – 7.31 (m, 8H), 7.28 (s, 1H), 7.15 (s, 1H), 7.04 – 6.96 (m, 2H), 6.26 – 6.15 (m, 1H), 5.14 (s, 2H), 3.85 (s, 2H), 3.61 (s, 2H), 3.22 (d, J = 3.8 Hz, 2H), 2.69 (d, J = 5.1 Hz, 2H), 2.64 (s, 2H). ^{13}C NMR (75 MHz, $CDCl_3$) δ 193.16, 164.27, 152.56, 137.11, 136.21, 135.72, 134.87, 134.15, 132.85, 131.88, 131.61, 130.92, 128.89, 128.46, 127.63, 126.22, 121.23, 115.96, 110.67, 70.48, 61.91, 53.82, 49.56, 32.07, 28.29. MS (ESI) m/z: calcd for

$C_{29}H_{26}BrNO_2$ $[M + H]^+$, 500.1; found, 500.1.

*(E)-5-(benzyloxy)-2-((1-(2-methylbenzyl)-1,2,3,6-tetrahydropyridin-4-yl)methylene)-2,3-dihydro-1H-inden-1-one(**B10**).* White solid, yield 42.6%, mp 122-124 °C. ^{1}H NMR (300 MHz, Chloroform-*d*) δ 7.81 (d, J = 8.4 Hz, 1H), 7.40 – 7.30 (m, 4H), 7.26 (s, 2H), 7.20 – 7.15 (m, 4H), 7.03 – 6.98 (m, 2H), 6.24 (s, 1H), 5.15 (s, 2H), 3.86 (s, 2H), 3.58 (s, 2H), 3.21 (s, 2H), 2.71 – 2.65 (m, 2H), 2.60 (s, 2H), 2.38 (s, 3H). ^{13}C NMR (75 MHz, $CDCl_3$) δ 193.16, 164.20, 152.61, 137.55, 136.51, 136.37, 136.24, 135.12, 134.15, 132.60, 131.89, 130.46, 129.81, 128.86, 128.42, 127.61, 127.29, 126.12, 125.74, 115.91, 110.62, 70.43, 60.40, 54.12, 49.71, 32.05, 28.45, 19.43. MS (ESI) m/z: calcd for $C_{30}H_{29}NO_2$ $[M + H]^+$, 436.2; found, 436.2.

*(E)-5-(benzyloxy)-2-((1-(3-methylbenzyl)-1,2,3,6-tetrahydropyridin-4-yl)methylene)-2,3-dihydro-1H-inden-1-one(**B11**).* White solid, yield 42.9%, mp 122-124 °C. ^{1}H NMR (300 MHz, Chloroform-*d*) δ 7.80 (d, J = 8.3 Hz, 1H), 7.46 – 7.34 (m, 5H), 7.15 (ddt, J = 23.5, 15.9, 7.4 Hz, 5H), 6.99 (d, J = 9.2 Hz, 2H), 6.23 (d, J = 3.9 Hz, 1H), 5.14 (s, 2H), 3.85 (s, 2H), 3.58 (s, 2H), 3.19 (d, J = 3.7 Hz, 2H), 2.66 (t, J = 5.2 Hz, 2H), 2.61 (s, 2H), 2.35 (s, 3H). ^{13}C NMR (75 MHz, $CDCl_3$) δ 193.10, 164.14, 152.50, 138.03, 137.86, 136.14, 134.99, 134.03, 132.58, 131.83, 129.94, 128.78, 128.34, 128.23, 128.04, 127.53, 127.52, 126.32, 126.08, 115.83, 110.56, 70.36, 62.67, 53.85, 49.57, 31.95, 28.25, 21.43. MS (ESI) m/z: calcd for $C_{30}H_{29}NO_2$ $[M + H]^+$, 436.2;

found, 436.2.

*(E)-5-(benzyloxy)-2-((1-(4-methylbenzyl)-1,2,3,6-tetrahydropyridin-4-yl)methylene)-2,3-dihydro-1H-inden-1-one(**B12**).* White solid, yield 44.2%, mp 124-126 °C. ^{1}H NMR (300 MHz, Chloroform-*d*) δ 7.78 (d, J = 8.3 Hz, 1H), 7.42 – 7.29 (m, 5H), 7.24 (d, J = 7.9 Hz, 2H), 7.19 – 7.10 (m, 3H), 7.03 – 6.91 (m, 2H), 6.19 (d, J = 3.8 Hz, 1H), 5.11 (s, 2H), 3.79 (s, 2H), 3.57 (s, 2H), 3.16 (d, J = 4.0 Hz, 2H), 2.63 (d, J = 5.1 Hz, 2H), 2.58 (d, J = 5.2 Hz, 2H), 2.34 (s, 3H). ^{13}C NMR (75 MHz, $CDCl_3$) δ 193.20, 164.27, 152.67, 137.05, 136.28, 135.09, 134.92, 134.17, 132.73, 131.94, 129.36, 129.22, 128.91, 128.47, 127.67, 126.17, 116.00, 110.67, 70.48, 62.47, 53.87, 49.60, 32.09, 28.37, 21.34. MS (ESI) m/z: calcd for $C_{30}H_{29}NO_2$ $[M + H]^+$, 436.2; found, 436.2.

*(E)-5-(benzyloxy)-2-((1-(2-(trifluoromethyl)benzyl)-1,2,3,6-tetrahydropyridin-4-yl)methylene)-2,3-dihydro-1H-inden-1-one(**B13**).* White solid, yield 46.2%, mp 124-126 °C. ^{1}H NMR (400 MHz, Chloroform-*d*) δ 7.82 (dd, J = 10.1, 7.9 Hz, 2H), 7.69 – 7.61 (m, 1H), 7.53 (t, J = 7.6 Hz, 1H), 7.46 – 7.38 (m, 4H), 7.38 – 7.32 (m, 2H), 7.18 (s, 1H), 7.05 – 6.96 (m, 2H), 6.24 (d, J = 3.8 Hz, 1H), 5.14 (s, 2H), 3.86 (s, 2H), 3.78 (s, 2H), 3.24 (q, J = 2.9 Hz, 2H), 2.68 (t, J = 5.6 Hz, 2H), 2.62 (d, J = 6.2 Hz, 2H). ^{13}C NMR (101 MHz, $CDCl_3$) δ 193.03, 164.12, 152.45, 136.11, 136.02, 134.85, 134.01, 132.64, 131.89, 131.79, 130.19, 128.76, 128.32, 127.51, 126.89, 126.06,

125.84, 125.78, 125.72, 125.66, 115.80, 110.54, 70.34, 57.72, 53.92, 49.74, 31.96, 28.36. MS (ESI) m/z: calcd for $C_{30}H_{26}F_3NO_2$ $[M + H]^+$, 490.2; found, 490.2.

*(E)-5-(benzyloxy)-2-((1-(3-(trifluoromethyl)benzyl)-1,2,3,6-tetrahydropyridin-4-yl)methylene)-2,3-dihydro-1H-inden-1-one(**B14**)*. White solid, yield 42.3%, mp 126-128 °C. ^{1}H NMR (300 MHz, Chloroform-*d*) δ 7.81 (d, J = 8.3 Hz, 1H), 7.63 (s, 1H), 7.55 (t, J = 7.7 Hz, 2H), 7.41 (q, J = 7.7 Hz, 6H), 7.17 (s, 1H), 7.00 (d, J = 10.0 Hz, 2H), 6.23 (d, J = 4.0 Hz, 1H), 5.14 (s, 2H), 3.85 (s, 2H), 3.66 (s, 2H), 3.20 (d, J = 3.8 Hz, 2H), 2.73 – 2.53 (m, 4H). ^{13}C NMR (75 MHz, $CDCl_3$) δ 193.03, 164.17, 152.46, 139.28, 136.11, 135.63, 134.74, 134.05, 132.76, 132.35, 131.77, 128.84, 128.77, 128.33, 127.51, 126.09, 125.65, 125.61, 124.17, 124.12, 115.85, 110.55, 70.35, 62.01, 53.81, 49.52, 31.95, 28.21. MS (ESI) m/z: calcd for $C_{30}H_{26}F_3NO_2$ $[M + H]^+$, 490.2; found, 490.2.

*(E)-5-(benzyloxy)-2-((1-(4-(trifluoromethyl)benzyl)-1,2,3,6-tetrahydropyridin-4-yl)methylene)-2,3-dihydro-1H-inden-1-one(**B15**)*. White solid, yield 42.8%, mp 124-126 °C. ^{1}H NMR (300 MHz, Chloroform-*d*) δ 7.81 (d, J = 8.4 Hz, 1H), 7.59 (d, J = 7.9 Hz, 2H), 7.49 (d, J = 8.0 Hz, 2H), 7.44 – 7.36 (m, 5H), 7.17 (s, 1H), 7.00 (dd, J = 11.2, 3.1 Hz, 2H), 6.23 (d, J = 3.9 Hz, 1H), 5.15 (s, 2H), 3.86 (s, 2H), 3.67 (s, 2H), 3.20 (d, J = 3.8 Hz, 2H), 2.65 (dd, J = 10.3, 6.0 Hz, 4H). ^{13}C NMR (75 MHz, $CDCl_3$) δ 193.04, 164.18, 152.44,

142.40, 136.10, 135.60, 134.74, 134.05, 132.76, 131.77, 129.21, 128.77, 128.34, 127.51, 126.11, 125.34, 125.29, 125.25, 115.84, 110.56, 70.36, 61.98, 53.83, 49.54, 31.95, 28.23. MS (ESI) m/z: calcd for $C_{30}H_{26}F_3NO_2$ $[M + H]^+$, 490.2; found, 490.2.

*(E)-5-(benzyloxy)-2-((1-(2-nitrobenzyl)-1,2,3,6-tetrahydropyridin-4-yl)methylene)-2,3-dihydro-1H-inden-1-one(**B16**)*. White solid, yield 40.2%, mp 124-126 °C. ^{1}H NMR (300 MHz, Chloroform-*d*) δ 7.89 – 7.77 (m, 2H), 7.67 (d, J = 8.0 Hz, 1H), 7.57 (td, J = 7.6, 1.3 Hz, 1H), 7.46 – 7.37 (m, 6H), 7.15 (s, 1H), 7.03 – 6.96 (m, 2H), 6.18 (d, J = 3.8 Hz, 1H), 5.14 (s, 2H), 3.91 (s, 2H), 3.84 (s, 2H), 3.25 – 3.18 (m, 2H), 2.63 (d, J = 5.2 Hz, 2H), 2.57 (d, J = 5.6 Hz, 2H). ^{13}C NMR (75 MHz, $CDCl_3$) δ 193.10, 164.15, 152.50, 149.67, 136.11, 135.77, 134.82, 134.00, 133.89, 132.69, 131.75, 130.86, 128.78, 128.35, 128.06, 127.55, 126.09, 124.59, 115.83, 110.54, 70.35, 58.56, 53.83, 49.75, 31.97, 28.21. MS (ESI) m/z: calcd for $C_{29}H_{26}N_2O_4$ $[M + H]^+$, 467.2; found, 467.2.

*(E)-5-(benzyloxy)-2-((1-(3-nitrobenzyl)-1,2,3,6-tetrahydropyridin-4-yl)methylene)-2,3-dihydro-1H-inden-1-one(**B17**).* White solid, yield 38.6%, mp 126-128 °C. ^{1}H NMR (400 MHz, Chloroform-*d*) δ 8.25 (t, J = 2.0 Hz, 1H), 8.14 (ddd, J = 8.2, 2.4, 1.1 Hz, 1H), 7.81 (d, J = 8.5 Hz, 1H), 7.76 – 7.70 (m, 1H), 7.51 (t, J = 7.9 Hz, 1H), 7.46 – 7.34 (m, 5H), 7.17 (d, J = 2.2 Hz, 1H), 7.05 – 6.96 (m, 2H), 6.22 (t, J = 3.9 Hz, 1H), 5.15 (s, 2H), 3.87 (s, 2H), 3.72

(s, 2H), 3.23 (q, *J* = 2.8 Hz, 2H), 2.69 (t, *J* = 5.5 Hz, 2H), 2.63 (d, *J* = 5.7 Hz, 2H). ^{13}C NMR (101 MHz, $CDCl_3$) δ 192.95, 164.14, 152.39, 148.39, 136.05, 134.98, 134.55, 134.03, 132.84, 131.71, 129.30, 128.73, 128.30, 127.47, 126.07, 123.69, 122.39, 115.82, 110.52, 70.33, 61.54, 53.71, 49.54, 31.92, 28.16. MS (ESI) m/z: calcd for $C_{29}H_{26}N_2O_4$ $[M + H]^+$, 467.2; found, 467.2.

*(E)-5-(benzyloxy)-2-((1-(4-nitrobenzyl)-1,2,3,6-tetrahydropyridin-4-yl)methylene)-2,3-dihydro-1H-inden-1-one(**B18**).* White solid, yield 37.9%, mp 124-126 °C. ^{1}H NMR (300 MHz, Chloroform-*d*) δ 8.19 (d, *J* = 8.6 Hz, 2H), 7.80 (d, *J* = 8.4 Hz, 1H), 7.55 (d, *J* = 8.5 Hz, 2H), 7.42 – 7.35 (m, 5H), 7.16 (s, 1H), 7.04 – 6.97 (m, 2H), 6.20 (d, *J* = 3.8 Hz, 1H), 5.14 (s, 2H), 3.85 (s, 2H), 3.71 (s, 2H), 3.21 (d, *J* = 3.5 Hz, 2H), 2.66 (d, *J* = 4.4 Hz, 2H), 2.62 (s, 2H). ^{13}C NMR (75 MHz, $CDCl_3$) δ 193.15, 164.35, 152.59, 147.41, 146.34, 136.22, 135.50, 134.75, 134.19, 133.01, 131.85, 129.64, 128.91, 128.49, 127.65, 126.25, 123.80, 116.03, 110.70, 70.51, 61.81, 53.98, 49.80, 32.09, 28.34. MS (ESI) m/z: calcd for $C_{29}H_{26}N_2O_4$ $[M + H]^+$, 467.2; found, 467.2.

Biological activity

In Vitro AChE inhibition assay.

A slightly modified Ellman assay was used to test the inhibitory effect of the target compound on AChE. An AChE solution (2U/mL) was prepared by dissolving AChE from Electrophorus electricus (C3389, Sigma-Aldrich) in 0.1 M phosphate buffer (pH 8.0). First, 20 μL of phosphate buffer (pH 8.0)

was dispensed into each well of a 96-well plate, followed by the addition of varying concentrations of test compounds (20 μL), 1 mM 5'-dithiobis (2-nitrobenzoic acid) (DTNB) solution (100 μL), and AChE solution (40 μL) in sequence. After incubating the plate at 37 ℃ for 15 minutes, a mixed solution was supplemented with 20 μL of acetylthiocholine iodide (1 mM). The absorbance of each plate at 405 nm was immediately recorded using a microplate reader (Thermo Scientific). The percentage inhibition of each compound was determined using the formula $(1 - Ai/Ac) \times 100$, where Ai and Ac represent the absorbance of AChE in the presence and absence of inhibitors, respectively. Each experiment was repeated thrice, and the IC_{50} values of all target compounds were calculated graphically using log concentration-percentage inhibition curves (Graph Pad Prism 8.0).

MAO-B Inhibition.

The inhibitory activity of the test compounds against MAO-B was evaluated by Amplex Red MAO assay using Human MAO-B purchased from Sigma-Aldrich (M7441). In brief, the test compounds were dissolved in 0.1 mL of sodium phosphate buffer (0.05 M, pH 7.4) and incubated with recombinant *h*MAO-B (0.75 μg/mL) for 15 minutes at 37°C in a flat-bottomed black-walled 96-well plate placed inside a dark fluorimeter chamber. Following the incubation period, the reaction was initiated by introducing Amplex Red

reagent (90101, Sigma-Aldrich) at a final concentration of 200 μM, horseradish peroxidase (P8375, Sigma-Aldrich) at a concentration of 1 U/mL and p-tyramine (T90344, Sigma-Aldrich) at a concentration of 1 mM. The results were analyzed from the fluorescence signal (excitation at 545 nm and emission at 590 nm) via a multi-detection microplate reader (MD5, Thermo Scientific). GraphPad Prism 8 was used to analyze the data, and the IC_{50} value was determined by fitting "single point competition" with the realized nonlinear regression.

Kinetic Characterization of AChE Inhibition.

The identical modified Ellman assay was employed to characterize the kinetics of acetylcholinesterase (AChE). In 96-well plates, each well was added with 20 μL of test compound **A1**, followed by 20 μL of acetylthiocholine iodide at varying concentrations (1.5−4 mM) and 20 μL of PBS. Finally, 40 μL of AChE was added to the mixture. After 15 minutes of incubation at 37°C, 100 μL of 0.1 mM DTNB was added and the absorbance of each plate was immediately recorded at 405 nm using a microplate reader (Thermo Scientific). The graph was evaluated by a weighted least squares analysis, where the variance of V was assumed to be a constant percentage of the whole dataset V. The concentration of test compounds was represented by

the slopes of these graphs, and Ki was calculated as the ratio of retest intercept to retest slope.

Molecular Docking Study.

3D crystal structures of AChE (PDB ID: 4EY7) and MAO-B (2V5Z) were retrieved from the Protein Data Bank (PDB, https://www.rcsb.org). The docking analysis was done with the help of Schrodinger software. AChE and MAO-B were refined using the protein preparation module and the compound **A1** and compound **B7** were prepared using the ligand preparation module. The docking site was generated with the receptor grid generation module. Finally, the ligand docking module was used to dock small molecules into the active pockets of AChE and MAO-B.

Cytotoxicity Assay on SH-SY5Y Cells.

The viability of human neuroblastoma SH-SY5Y cells was assessed using the 3-(4,5-dimethylthiazol-2-yl)-2,5-diphenyl-tetrazolium bromide (MTT) assay. SHSY5Y cells were cultured in a 25 cm^2 flask with fresh MEM/F12 medium supplemented with 10% fetal bovine serum, 100 U/mL penicillin, and 100 g/mL streptomycin. The culture was maintained at 37 °C under a humidified atmosphere of 5% CO_2. Cells were seeded in a 96-well plate at a density of 1×10^4 cells per well. After 24 hours of culture, the medium was removed and

compounds **A1** (at concentrations of 10, 25, and 50 μM) were prepared in serum-free media and added to each well of the plate. Following a treatment period of another 24 hours, each well received a solution containing 10 mL of the compound 3-(4,5-dimethyl-2-thiazolyl)-2,5-diphenyl-2-*H*-tetrazolium bromide. Following a 4-hour incubation at 37°C, 100 μL DMSO was added to dissolve the formazan crystals. Finally, we recorded the absorbance of the resulting mixture at 490 nm via the microplate reader (FC/K3, Thermo, Waltham, MA, USA). The formula for calculating the survival rate was Ae/Ab×100%, where Ae and Ab respectively denote the absorbance of SH-SY5Y cells in the presence and absence of target drugs.

DPPH radical-scavenging potency.

Compound **A1** was evaluated for its antioxidant activity by scavenging the 2,2-diphenyl-1-picrylhydrazyl (DPPH) radical using a modified protocol based on Blois' method. A concentration of 50 μM of the test compound was mixed with a methanol solution of 1 mM in 0.1 mL DPPH at room temperature, resulting in a total reaction mixture volume of 3 mL. The reactions were conducted in 96-well microplates, each containing 200μL of the final reaction mixture. Following the addition of test compounds to 0.1mM DPPH, the mixture was agitated at 37°C for one minute and subsequently incubated in darkness for thirty minutes. Trolox was used as a reference. The absorbance

was quantified at 517nm using a microplate reader. The experiments were conducted in triplicate, and the blank value (compound without DPPH) was subtracted. The ability of the tested compounds to scavenge DPPH radicals was determined using the following equation:

DPPH scavenging effect(%)=(Ac-As)/Ac×100

Where AC represents the absorbance of the control (DPPH radical solution in methanol), and AS denotes the absorbance value of the sample (solution containing DPPH radical and tested compound in methanol).

Morris water maze test was conducted on mice induced with scopolamine.

Experimental subjects were adult female ICR mice (8-10 weeks old, weighing 25-30 g) obtained from Shanghai, China. Divide the mice into four groups according to the random number table method: (i) control group (physiological saline); (ii) Model group (scopolamine); (iii) Compound group (scopolamine+**A1**); (iv) Positive group (scopolamine + donepezil). The experiment spanned 16 days and was partitioned into two phases: (1) Injection phase (days 1-10): where donepezil, **A1** (10 mg/kg), or saline was administered intraperitoneally once daily for 10 consecutive days, followed by scopolamine solution (5 mg/kg) thirty minutes later. (2) Exploration phase (days 11-16): the water maze was situated in a dimly lit room at a temperature of 25 ℃. The circular pool (with a diameter of 120 centimeters and a height

of 60 centimeters) is evenly divided into four quadrants. At the center of the fourth quadrant, there is an escape platform with a diameter of 10 cm and a water depth of 40 cm. The behavioral study of each mouse included learning and memory training on days 11-14 and cognitive behavioral assessment on day 16, during which appropriate drugs were injected daily. The mice were introduced into the pool and proceeded to locate the platform. Each mouse underwent training once in each of the four quadrants of the pool (days 11-14) for a duration of 90s, during which the latency to locate and reach the platform was recorded as an indicator of successful escape. If the mice failed to reach the platform within 90 s, they will be guided to the platform to terminate the test. The mice were placed on the platform for a duration of 10 s, regardless of whether they successfully reached it within the allotted time frame of 90 s. On the final day (day 16), mice underwent an exploratory experiment involving water entry from the second quadrant, during which they were given a 90s limit to locate the platform. The ANY-maze video tracking system was utilized to record data on the time of arrival at the missing platform, the number of platform crossings, and escape latency. The collected data was then analyzed and processed using GraphPad Prism 8.0 software.

Inhibition of self-mediated Aβ$_{1-42}$ aggregation.

The inhibition of self-mediated aggregation of Aβ_{1-42} was assessed through a

Thioflavin T (ThT)-binding assay. A$\beta_{1\text{-}42}$ was initially dissolved in 1,1,1,3,3,3-hexafluoro-2-propanol (HFIP) through brief sonication for 10 minutes and subsequently left to stand at room temperature overnight. Subsequently, the HFIP was evaporated under a vacuum to remove it. The HFIP-pretreated A$\beta_{1\text{-}42}$ samples were reconstituted in DMSO and a 10 mM phosphate buffer (pH 7.4) to obtain a stable stock solution with A$\beta_{1–42}$ concentration of 50 μM. To inhibit self-mediated A$\beta_{1\text{-}42}$ aggregation, a mixture of the peptide (20 μL, final concentration 25 μM) with or without the inhibitor (20 μL, final concentration 20 μM) was incubated in darkness at 37°C for 24 h. To disaggregate self-mediated A$\beta_{1\text{-}42}$ aggregation, the peptide was initially incubated in darkness at 37°C for 24 h. Subsequently, the inhibitor was added and the mixture was further incubated under identical conditions for another 24 h. Following incubation, 20 μL of the sample was transferred to a black 96-well plate and diluted with 50 μM gly-NaOH buffer (pH 8.5) containing 5 μL ThT to a final volume of 200 μL. The fluorescence intensities of each inhibitor were measured in triplicate at 450 nm (λex) and 485 nm (λem). The percentage of inhibition on aggregation was calculated by the following expression: $(1-IF_i/IF_c)*100\%$ in which IF_i and IF_c were the fluorescence intensities obtained for absorbance in the presence and absence of inhibitors, respectively, after subtracting the fluorescence of respective blanks.

Results & discussion

Chemistry

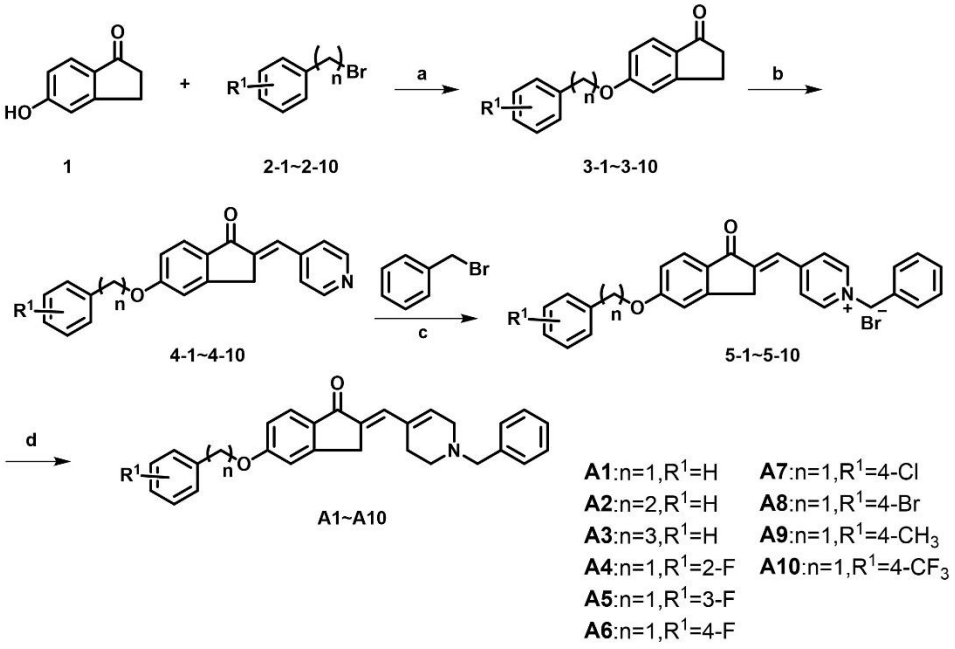

Figure 2. Synthetic Protocol for the Synthesis of Compounds **A1** ~ **A10.** Reagents and conditions: (a) dry DMF, 65℃, 1-3 h; (b) 4-pyridinecarboxaldehyde, *p*-toluenesulfonic acid monohydrate, toluene, reflux, 4 h; (c) dry MeCN, reflux, 1-3 h; (d) $NaBH_4$, MeOH, 0℃, 1h.

We used 5-hydroxy-1-indanone as the starting material and obtained intermediates **3** by nucleophilic substitution with compounds **2** with different substitutions. Intermediate **3** and 4-pyridinecarboxaldehyde underwent an aldol condensation reaction to yield intermediates **4**. Intermediates **5** were obtained by reacting intermediate **4** with benzyl bromide under reflux conditions in acetonitrile, followed by reduction with sodium borohydride to yield the target compounds **A1-A10**. The synthetic procedure for the target compounds **B1-B18** was illustrated in Figure 3, which follows a similar methodology as depicted in Figure 2.

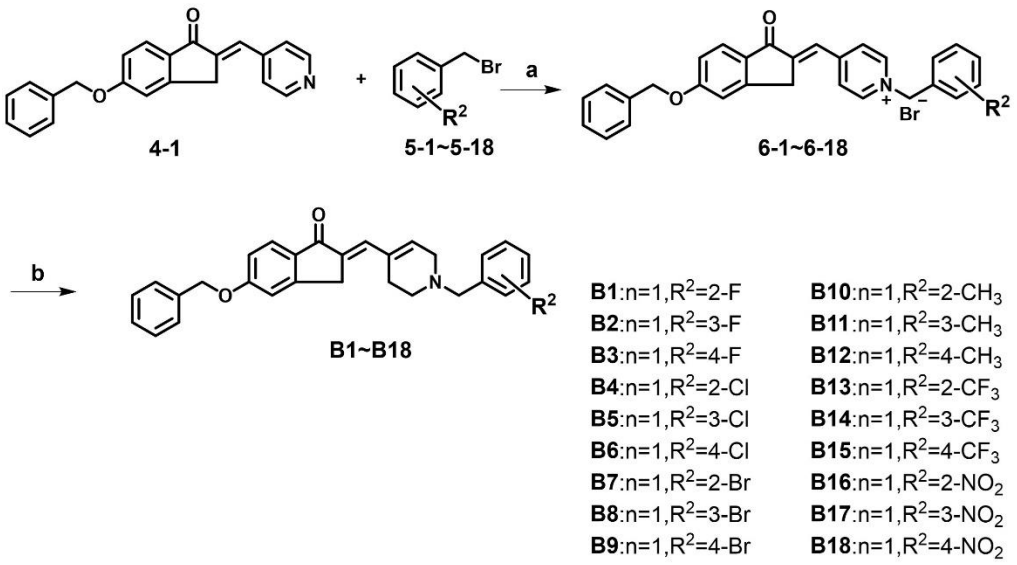

Figure 3. Synthetic Protocol for the Synthesis of Compounds **B1** ~ **B18**. Reagents and conditions: (a) dry MeCN, reflux, 1-3 h; and (d) $NaBH_4$, 0°C, 1 h.

Structure−Activity Relationship Analysis. The AChE inhibitory activity was investigated by electrophorus electricus AChE (*ee*AChE) using modified Ellman's method. The AChE inhibitory activity of all compounds during optimizations was tested using donepezil as a reference. The MAO-B inhibitory activity was explored by measuring the effects on the production of hydrogen peroxide from *p*-tyramine, with pargyline as the corresponding positive control. The results of the preliminary bioassay in Table 1 demonstrated that most of the indanones derivatives**(A1-A10)** exhibited potent inhibitory activity against AChE and some of them had good inhibitory activity against MAO-B.

In the first round of structural optimization, the B region of the compound **A1** was retained, while the length of the link between the A ring and the core was changed and the phenyl ring located in the A region was

modified by various substituents. As shown in Table 1, the inhibitory activity of the indanones derivatives against AChE and MAO-B decreased with the increase of the link length (**A1 > A2 > A3**). When introducing fluorine to the A ring, the influence on activity was *para-* > *ortho-* > *meta-* (**A6 > A4 > A5**). Subsequently, the introduction of 4-Cl or 4-Br to the A ring resulted in a significant reduction in enzyme inhibition potency compared to **A1** (**A1 > A6 > A7 > A8**), suggesting that halogen substituents wouldn't contribute to the activity. Finally, when 4-CH_3 and 4-CF_3 were substituted (**A9** and **A10**), the inhibitory activity against AChE and MAO-B both decreased. To summarize, introducing substituents in the A ring decreased the potency of inhibition to the two enzymes in varying degrees, especially to MAO-B. Therefore, the compound **A1** with the best activity was chosen as the lead for the second round of modifications.

In the second round of structural optimization, we kept the A region unchanged and explored the effect of the R2 substituent on the B ring. The substituent position optimization showed that the potency of the compound with a fluorine substituent was *meta-* > *ortho-* > *para-* (**B2 > B1 > B3**), the same as Cl, Br, CH_3, CF_3 and NO_2 substituents. When the substituent was a halogen, the order of activity was 3-Cl > 3-F > 3-Br (**B5 > B2 > B8**). When the 3-CH_3 (**B11**)，electron-donating group， was introduced to the B ring，the inhibitory activity of AChE and MAO-B decreased twofold. Introducing

the 3-NO_2 (**B17**), electron-withdrawing group, to the B ring decreased the inhibitory activity against AChE and did not influence MAO-B. In conclusion, the studies conducted so far have allowed us to obtain complete structure-activity relationships (SAR) for all compounds (Figure S1). Compounds without substituents on the benzene ring may be the potential dual AChE/ MAO-B inhibitors.

After these exploration on structural optimization, compound **A1** showed the best inhibitory activity for AChE and MAO-B (*ee*AChE: IC_{50} = 0.054 ± 0.004μM; MAO-B: IC_{50}=3.25 ± 0.20μM).

Table 1. Inhibition of AChE and MAO-B

Compound	*ee*AChE IC_{50} (μM)[a]	MAO-B IC_{50} (μM)[a]
A1	0.054 ± 0.004	3.25 ± 0.20
A2	0.123 ± 0.013	32.3 ± 2.5
A3	0.092 ± 0.014	120.2 ± 9.3
A4	0.073 ± 0.009	28.1 ± 2.4
A5	0.127 ± 0.013	32.9 ± 4.7
A6	0.086 ± 0.012	26.0 ± 3.2
A7	0.233 ± 0.027	43.5 ± 2.6
A8	0.115 ± 0.009	81.6 ± 4.1
A9	0.089 ± 0.018	18.8 ± 1.7
A10	0.132 ± 0.009	21.6 ± 2.9
B1	0.102 ± 0.016	42.7 ± 2.6

B2	0.029 ± 0.005	33.6 ± 3.3
B3	0.148 ± 0.018	25.5 ± 2.9
B4	0.094 ± 0.017	14.0 ± 2.8
B5	0.061 ± 0.011	12.3 ± 1.6
B6	0.81 ± 0.09	8.5 ± 1.5
B7	8.1 ± 0.9	45.3 ± 3.5
B8	0.159 ± 0.035	22.2 ± 1.8
B9	15.2 ± 1.2	11.2 ± 1.7
B10	0.230 ± 0.021	80.2 ± 3.7
B11	0.107 ± 0.012	6.8 ± 2.4
B12	3.9 ± 0.4	5.7 ± 1.6
B13	0.755 ± 0.036	98.2 ± 4.8
B14	0.299 ± 0.023	5.5 ± 1.2
B15	18.3 ±2.5	3.8 ± 0.3
B16	1.6 ± 0.4	5.3 ± 0.6
B17	0.123 ± 0.015	3.6 ± 0.4
B18	33.0 ± 2.8	3.1 ± 0.3
Donepezil	0.038 ± 0.012	
Pargyline		0.023 ± 0.006

[a]Results are expressed as the mean of at least three experiments.

Kinetic Study of AChE. The Lineweaver Burk plot is a graphical representation of enzyme kinetics which is extensively used in the study of the mechanism of inhibitors against the corresponding enzymes. In the

enzyme kinetics study, compound **A1** was selected as the representative compound of the indanones derivatives to acquire the steady-state inhibition data. As demonstrated in Figure 4, with the increase in concentration, both slope and intercept showed an increasing trend, which revealed a mixed inhibition mechanism. The above results confirmed that the idanone derivatives bound to catalytic and peripheral sites of AChE at the same time for effective AChE inhibition.

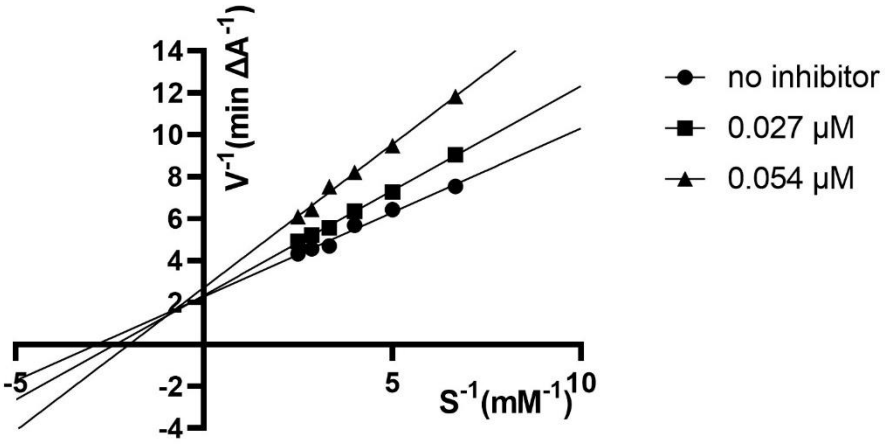

Figure 4. Lineweaver−Burk plot on two distinct concentrations of **A1** for AChE.

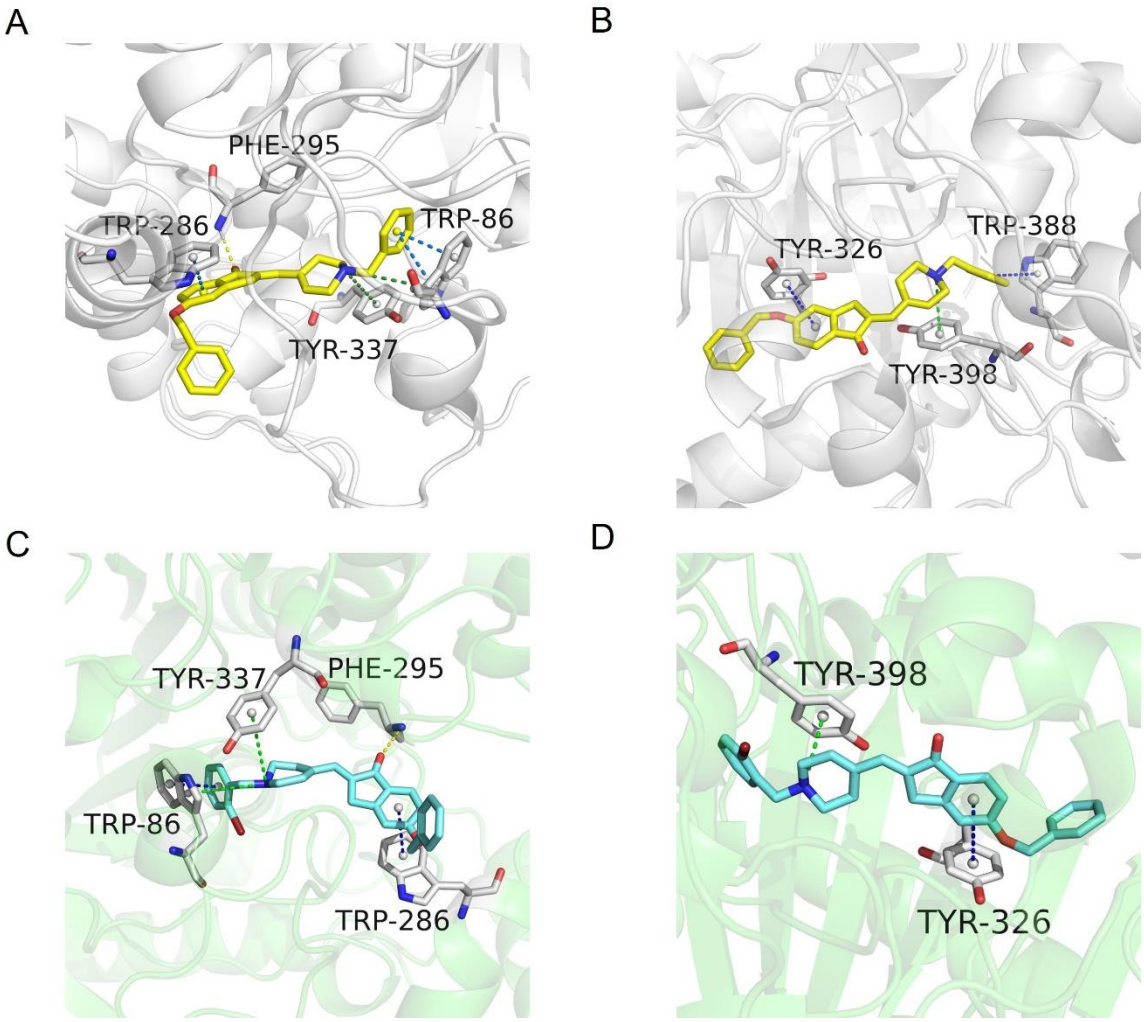

Figure 5. Predictive binding modes of compound **A1** (yellow stick) and compound **B7** (blue stick) with AChE (PDB code: 4EY7) and MAO-B (PDB code: 2V5Z), respectively. (A) The proposed binding mode of AChE in complex with compound **A1**; (B) The proposed binding mode of MAO-B in complex with compound **A1**; (C) The proposed binding mode of AChE in complex with compound **B7**; (D) The proposed binding mode of MAO-B in complex with compound **B7.** The hydrogen bonds, π–cation bonds, and π–π stacking contacts are shown as yellow, green, and blue dashed lines, respectively.

Molecular Modeling Simulations. In order to investigate the molecular mechanisms underlying the multitarget strategy, compound **A1** and compound **B7** were docked into the binding pockets of AChE (PDB code: 4EY7) and MAO-B (PDB code: 2V5Z) (Figure 5), respectively. The docking results showed that compound **A1** had a strong binding affinity with human

acetylcholinesterase with a docking score of −16.450 kcal/mol. As shown in Figure 5, the compound **A1** mainly interacted with the CAS and the PAS of AChE through six secondary bonds. In detail, the benzene ring of the Indanones fragment and the benzyl ring connected to the pyridine ring interact with Trp286 and Trp86 via the π–π stacking interaction respectively. Also, the carbonyl group involved in the H-bonding interaction with Phe295 and the N atom of the pyridine ring formed two π–cation interactions with Trp86 and Trp337. The docking results confirmed that compound **A1** can simultaneously bind to the PAS and CAS of AChE, which is consistent with the results of the kinetic study. To identify interactions between indanones derivates and MAO-B, we explored the docking model of compound **A1** with MAO-B. As shown in Figure 5, the Tyr398 residue from MAO-B formed a π–cation interaction with the N atom of the pyridine ring, and the benzene ring of the Indanones fragment and the benzyl ring connected to the pyridine ring interact with Tyr326 and Trp388 via the π–π stacking interaction respectively, which are considered vital to stabilize the compound in this binding pocket.

After investigating the binding pockets of AChE with compound **B7**, it was observed that compound **B7** lacks a π–π stacking interaction in comparison to compound **A1**. Simultaneously, an examination of the binding pockets of compound **B7** with MAO-B revealed a deficiency in π–π stacking interaction when compared to compound **A1**. We believe that the superior

binding affinity of compound **A1** to the pockets of AChE and MAO-B can be attributed precisely to the absence of substitutions on the benzene ring.

Therefore, the above results suggested that compound **A1** exhibited as an effective dual AChE/MAO-B inhibitor owing to the occupancy of the binding pockets and the interactions with the crucial residues in the enzymatic cavities.

Neurotoxicity Studies in SH-SY5Y Cells. To investigate whether **A1** had neurotoxicity, the 3-(4,5-dimethylthiazol-2-yl)-2,5-diphenyl-tetrazolium bromide (MTT) assay, assessing the viability of human neuroblastoma SH-SY5Y cells at three doses, was performed. The results exhibited a slightly decreasing cell viability at higher doses (Table S1). Fortunately, neuroblastoma SH-SY5Y cells still showed high cell viability (87 ± 0.34%) when exposed to compound **A1** at the maximum dose of 50 μM, suggesting that compound **A1** had little or no toxicity to SH-SY5Y neuroblastoma cells.

Table 2. Inhibition of A$\beta_{1\text{-}42}$ self-mediated aggregation and DPPH radical by compound **A1**.

Compound	A$\beta_{1\text{-}42}$ aggregation inhibition (%)[a]	Reduced DPPH(%)[b]
A1	23.60%	17.38%
Donepezil	4.86%	5.02%
Resveratrol	87.01%	72.41%
Trolox		83.18%

a: To inhibit the self-mediated aggregation of A$\beta_{1\text{-}42}$, the Thioflavin-T fluorescence method was employed and measurements were conducted in the presence of 25 μM compounds. The mean ± SD values were obtained from at least three independent experiments.
b: Compound **A1** was tested at 50μM compounds for evaluating its DPPH. Trolox was used as a reference.

Effects of A1 on Self-Mediated A$\beta_{1\text{-}42}$ Aggregation. The accumulation of Aβ causes oxidative stress and inflammation, leading to neurodegeneration[36]. Thus, the inhibition of Aβ aggregation in the brain represents a promising therapeutic strategy for AD. Compound **A1** was tested in vitro for inhibition of self-mediated A$\beta_{1\text{-}42}$ aggregation using the Thioflavin T (ThT) fluorometric assay, with resveratrol as the reference compound. The formation of amyloid plaques is attributed to an increase in the production and accumulation of A$\beta_{1\text{-}42}$ peptide, which subsequently oligomerizes and deposits as senile plaques[37]. Results showed that compound **A1** had moderate inhibitory effects on self-mediated Aβ aggregation at 25 μM (Table 2). In addition, we found that **A1** was more potent than donepezil in inhibiting self-mediated Aβ aggregation, which might be related to the CAS and PAS dual binding of AChE.

Antioxidant Activity and DPPH Assay. Deterioration of Oxidative stress is a progressive and inevitable process associated with aging that helps drive the progression of late-onset AD[38]. Therefore, scavenging oxygen-free radicals may be an effective strategy to prevent AD. As shown in Table 2, compound **A1** possessed moderate antioxidant activity at a concentration

of 25 μM in 1,1-diphenyl-2-picrylhydrazine radical scavenging activity (DPPH) assay.

ADMET Prediction of all Compounds. The absorption, distribution, metabolism, elimination, and toxicity (ADMET) properties of drug candidates are important for their efficacy and safety as therapeutics. We used ADMET Lab 2.0 (https://admetmesh.scbdd.com/) to predict the ADMET properties of all compounds. Table S2 showed that these compounds were likely to be smoothly absorbed into the small intestine after oral administration and had moderate blood−brain barrier penetration and clearance. Cytochrome P450 2C9 (CYP2C9) is one of the most important drugs metabolizing enzymes, and inhibition of CYP2C9 may lead to undesirable drug−drug interactions or drug toxicity. The results indicated that most of these compounds are noninhibitors of CYP2C9. In addition, AMES and rat acute toxicity studies showed that these compounds are predicted to have little to no toxic hazard.

Behavioral Studies in the AD Mice Model. To investigate the in vivo effects of candidate **A1**, the Morris water-maze test (MWM) was performed on the scopolamine (Scop) -induced AD mice, donepezil as positive controls. Briefly, 32 female ICR adult mice were randomly allocated into 4 groups (n = 8 for each group): control, Scop (model), Scop + **A1** (10 mg/kg), and Scop + donepezil (10 mg/kg). The mice from each group were treated with corresponding drug dosages by intraperitoneal injection for 10 consecutive

days. Each mouse received one learning and memory training session daily for 4 days before a cognitive behavioral test. Figure 6 showed that the Scop group significantly increased the escape latency of the target ($P<0.001$) and the travel distance ($P<0.01$) more than the control group (saline injection group). Compound **A1** exhibited superior efficacy compared to donepezil in rescuing the escape latency and distance to target induced, improving cognitive and memory impairment due to scopolamine-induced cholinergic deficit in mice (Figure 6). Therefore, compound **A1** could significantly improve spatial learning and cognition functions.

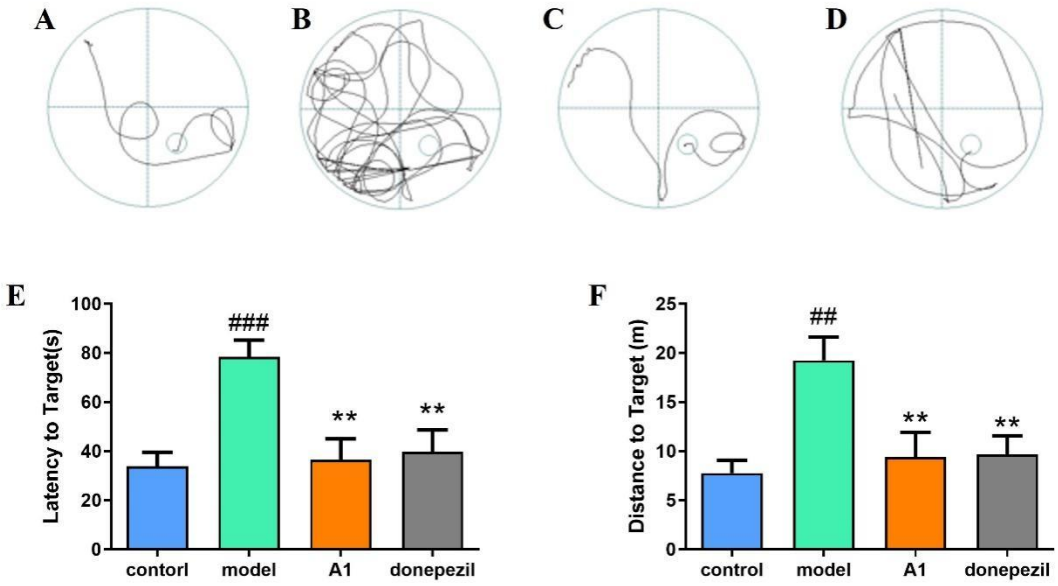

Figure 6. Anti-AD effects of intraperitoneal injection of **A1** (10 mg/kg), and donepezil (10 mg/kg), on scopolamine-induced cognitive impairment in ICR mice were determined by the MWM test. The trajectories of mice were shown as (A) control, (B) model, (C) **A1**, (D) donepezil groups, (E)latency to target, and (F) distance to the target. Data were presented as the mean ± SEM (n = 8; #P < 0.05, ##P < 0.01, ###P < 0.01 control group vs scopolamine model group; *P < 0.05, **P < 0.01, **A1** or donepezil group vs scopolamine model group).

Conclusion

AD is the third leading cause of disability and death in the elderly after cardiovascular and cerebrovascular diseases and malignant tumors. The pathogenesis of AD is complex, and the therapeutic effect of single-target drugs on AD is limited. Therefore, MTDLs may be an effective strategy for the design of new AD drugs. In this study, we have developed a series of dual AChE/MAO-B inhibitors that incorporated the pharmacophores of MTDLs **C10** with the chromanone moiety and the MAO-B inhibitor **2a**. The optimal compound **A1** exhibited good AChE and MAO-B dual inhibitory effects and moderate antioxidant activity. Molecular docking and kinetic studies had shown that **A1** can bind both CAS and PAS active sites of AChE. **A1** showed moderate inhibitory effects on self-mediated Aβ aggregation and very low toxicity to SH-SY5Y neuroblastoma cells. Importantly, *in vivo,* mouse model studies showed that **A1** significantly improved the cognitive and memory impairment caused by the scopolamine-induced cholinergic deficit. Taken together, **A1** exhibits potential as a lead of MTDL to develop new drugs for the treatment of AD.

Summary points

- The treatment of Alzheimer's disease (AD) is a formidable challenge due to its deleterious impact on memory and executive functions, which

significantly impede daily activities.

Experimental section

- Through a multitarget strategy, a series of novel indanone-1-benzyl-1,2,3,6-tetrahydropyridin derivatives were designed, synthesized and evaluated as the potential dual AChE/MAO-B inhibitors for Alzheimer's disease.

Results & discussion

- Compound **A1** exhibited the most potent inhibitory activity against both AChE and MAO-B (*ee*AChE: IC_{50} = 0.054 ± 0.004μM; MAO-B: IC_{50}=3.25 ± 0.20μM).
- Molecular docking and kinetic studies have demonstrated that **A1** can bind both CAS and PAS active sites of AChE.
- *In vivo*, mouse model studies have demonstrated that **A1** significantly ameliorates the cognitive and memory impairment induced by scopolamine-induced cholinergic deficit.

Conclusion

- The collective findings indicated that compound **A1** holds great potential as a promising lead of anti-AD drug for further development.

Supplementary data

Financial & competing Interests disclosure

References

Papers of special note have been highlighted as: • of interest; •• of considerable interest

1. Scheltens P, Blennow K, Breteler MMB, *et al.* Alzheimer's disease. *The Lancet*. 388(10043), 505–517 (2016).

• This reference mainly discusses the challenging treatment of Alzheimer's disease.

2. Rajasekhar K, Govindaraju T. Current progress, challenges and future prospects of diagnostic and therapeutic interventions in Alzheimer's disease. *RSC Adv.* 8(42), 23780–23804 (2018).

3. Selkoe DJ, Hardy J. The amyloid hypothesis of Alzheimer's disease at 25 years. *EMBO Molecular Medicine*. 8(6), 595–608 (2016).

4. Bloom GS. Amyloid-β and Tau: The Trigger and Bullet in Alzheimer Disease Pathogenesis. *JAMA Neurology*. 71(4), 505–508 (2014).

5. Lansdall CJ. An effective treatment for Alzheimer's disease must consider both amyloid and tau. *Bioscience Horizons: The International Journal of Student Research*. 7, hzu002 (2014).

6. Barnham KJ, Bush AI. Biological metals and metal-targeting compounds

in major neurodegenerative diseases. *Chem. Soc. Rev.* 43(19), 6727–6749 (2014).

7. Anne Eckert, Schmitt K, Götz J. Mitochondrial dysfunction - the beginning of the end in Alzheimer's disease? Separate and synergistic modes of tau and amyloid-β toxicity. *Alzheimer's Research & Therapy*. 3(2), 15 (2011).

8. Zhang P, Xu S, Zhu Z, Xu J. Multi-target design strategies for the improved treatment of Alzheimer's disease. *European Journal of Medicinal Chemistry*. 176, 228–247 (2019).

9. Li X, Li T, Zhang P, *et al.* Discovery of novel hybrids containing clioquinol−1-benzyl-1,2,3,6-tetrahydropyridine as multi-target-directed ligands (MTDLs) against Alzheimer's disease. *European Journal of Medicinal Chemistry*. 244, 114841 (2022).

10. Zotova E, Nicoll JA, Kalaria R, Holmes C, Boche D. Inflammation in Alzheimer's disease: relevance to pathogenesis and therapy. *Alzheimers Res Ther*. 2(1), 1 (2010).

11. Perry VH, Holmes C. Microglial priming in neurodegenerative disease. *Nat Rev Neurol*. 10(4), 217–224 (2014).

12. Steele JW, Fan E, Kelahmetoglu Y, Tian Y, Bustos V. Modulation of Autophagy as a Therapeutic Target for Alzheimer's Disease. *Postdoc J*. 1(2), 21–34 (2013).

13. Zare-shahabadi A, Masliah E, Johnson GVW, Rezaei N. Autophagy in Alzheimer's disease. *Reviews in the Neurosciences*. 26(4), 385-395 (2015).

14. Wiesner J, Kříž Z, Kuča K, Jun D, Koča J. Acetylcholinesterases – the structural similarities and differences. *Journal of Enzyme Inhibition and Medicinal Chemistry*. 22(4), 417–424 (2007).

15. van Greunen DG, Johan van der Westhuizen C, Cordier W, *et al.* Novel *N*-benzylpiperidine carboxamide derivatives as potential cholinesterase inhibitors for the treatment of Alzheimer's disease. *European Journal of Medicinal Chemistry*. 179, 680–693 (2019).

16. Yao H, Uras G, Zhang P, *et al.* Discovery of Novel Tacrine–Pyrimidone Hybrids as Potent Dual AChE/GSK-3 Inhibitors for the Treatment of Alzheimer's Disease. *J. Med. Chem.* 64(11), 7483–7506 (2021).

17. Vitek GE, Decourt B, Sabbagh MN. Lecanemab (BAN2401): an anti–beta-amyloid monoclonal antibody for the treatment of Alzheimer disease. *Expert Opinion on Investigational Drugs*. 32(2), 89–94 (2023).

18. Zhou B, Lu JG, Siddu A, Wernig M, Südhof TC. Synaptogenic effect of APP -Swedish mutation in familial Alzheimer's disease. *Sci. Transl. Med*. 14(667), eabn9380 (2022).

19. Kumar B, Sheetal S, Mantha AK, Kumar V. Recent developments on the structure–activity relationship studies of MAO inhibitors and their role in different neurological disorders. *RSC Adv.* 6(48), 42660–42683 (2016).

20. Binda C, Newton-Vinson P, Hubálek F, Edmondson DE, Mattevi A. Structure of human monoamine oxidase B, a drug target for the treatment of neurological disorders. *Nat Struct Mol Biol*. 9(1), 22–26 (2002).

21. De Colibus L, Li M, Binda C, Lustig A, Edmondson DE, Mattevi A. Three-dimensional structure of human monoamine oxidase A (MAO A): Relation to the structures of rat MAO A and human MAO B. *Proc. Natl. Acad. Sci. U.S.A.* 102(36), 12684–12689 (2005).

22. Finberg JPM. Update on the pharmacology of selective inhibitors of MAO-A and MAO-B: Focus on modulation of CNS monoamine neurotransmitter release. *Pharmacology & Therapeutics*. 143(2), 133–152 (2014).

23. Pisani L, Catto M, Leonetti F, *et al.* Targeting Monoamine Oxidases with Multipotent Ligands: An Emerging Strategy in the Search of New Drugs

Against Neurodegenerative Diseases. *CMC*. 18(30), 4568–4587 (2011).

•• This reference explains that MAO-B inhibitors can be used to treat neurodegenerative diseases.

24. Emilsson L, Saetre P, Balciuniene J, Castensson A, Cairns N, Jazin EE. Increased monoamine oxidase messenger RNA expression levels in frontal cortex of Alzheimer's disease patients. *Neuroscience Letters*. 326(1), 56–60 (2002).

25. Chan HH, Tse MK, Kumar S, Zhuo L. A novel selective MAO-B inhibitor with neuroprotective and anti-Parkinsonian properties. *European Journal of Pharmacology*. 818, 254–262 (2018).

26. Reis J, Fernandes C, Salem H, *et al.* Design and synthesis of chromone-based monoamine oxidase B inhibitors with improved drug-like properties. *European Journal of Medicinal Chemistry*. 239, 114507 (2022).

27. Manzoor S, Hoda N. A comprehensive review of monoamine oxidase inhibitors as Anti-Alzheimer's disease agents: A review. *European Journal of Medicinal Chemistry*. 206, 112787 (2020).

•• This reference explains that novel multi-target design strategies (MTDLs) may be an effective treatment method for Alzheimer's disease.

28. Agis-Torres A, Sollhuber M, Fernandez M, Sanchez-Montero JM. Multi-Target-Directed Ligands and other Therapeutic Strategies in the Search of a Real Solution for Alzheimer's Disease. *CN*. 12(1), 2–36 (2014).

29. Carradori S, Ortuso F, Petzer A, *et al.* Design, synthesis and biochemical evaluation of novel multi-target inhibitors as potential anti-Parkinson agents. *European Journal of Medicinal Chemistry*. 143, 1543–1552 (2018).

30. Kumar B, Kumar V, Prashar V, *et al.* Dipropargyl substituted diphenylpyrimidines as dual inhibitors of monoamine oxidase and acetylcholinesterase. *European Journal of Medicinal Chemistry*. 177, 221–234 (2019).

31. Xie S-S, Wang X, Jiang N, *et al.* Multi-target tacrine-coumarin hybrids: Cholinesterase and monoamine oxidase B inhibition properties against Alzheimer's disease. *European Journal of Medicinal Chemistry*. 95, 153–165 (2015).

32. Sterling J, Herzig Y, Goren T, *et al.* Novel Dual Inhibitors of AChE and MAO Derived from Hydroxy Aminoindan and Phenethylamine as Potential Treatment for Alzheimer's Disease. *J. Med. Chem.* 45(24), 5260–5279 (2002).

•• This reference elaborates on MAO-B inhibitors with indan-1-one structure as the backbone.

33. Mostert S, Petzer A, Petzer JP. Indanones As High-Potency Reversible Inhibitors of Monoamine Oxidase. *ChemMedChem*. 10(5), 862–873 (2015).

•• This reference reports a new chromanone derivative C10, which is an AChE/MAO-B inhibitor.

34. Li X, Li T, Zhan F, *et al.* Design, Synthesis, and Biological Evaluation of Novel Chromanone Derivatives as Multifunctional Agents for the Treatment of Alzheimer's Disease. *ACS Chem. Neurosci.* 13(23), 3488–3501 (2022).

35. Zhang H, Wang Y, Wang Y, Li X, Wang S, Wang Z. Recent advance on carbamate-based cholinesterase inhibitors as potential multifunctional agents against Alzheimer's disease. *European Journal of Medicinal Chemistry*. 240, 114606 (2022).

36. Jiang N, Li S-Y, Xie S-S, *et al.* Design, synthesis and evaluation of multifunctional salphen derivatives for the treatment of Alzheimer's disease. *European Journal of Medicinal Chemistry*. 87, 540–551 (2014).

37. Umar T, Shalini S, Raza MK, *et al.* A multifunctional therapeutic

approach: Synthesis, biological evaluation, crystal structure and molecular docking of diversified 1H-pyrazolo[3,4-b]pyridine derivatives against Alzheimer's disease. *European Journal of Medicinal Chemistry*. 175, 2–19 (2019).

38. Jiang T, Sun Q, Chen S. Oxidative stress: A major pathogenesis and potential therapeutic target of antioxidative agents in Parkinson's disease and Alzheimer's disease. *Progress in Neurobiology*. 147, 1–19 (2016).